Studies of Thermal Stability of Multivalent DNA Hybridization in a Nanostructured System

Jeanette Nangreave, Hao Yan,* and Yan Liu*
Department of Chemistry and Biochemistry and the Biodesign Institute, Arizona State University, Tempe, Arizona

ABSTRACT A fundamental understanding of molecular self-assembly processes is important for improving the design and construction of higher-order supramolecular structures. DNA tile based self-assembly has recently been used to generate periodic and aperiodic nanostructures of different geometries, but there have been very few studies that focus on the thermodynamic properties of the inter-tile interactions. Here we demonstrate that fluorescently-labeled multihelical DNA tiles can be used as a model platform to systematically investigate multivalent DNA hybridization. Real-time monitoring of DNA tile assembly using fluorescence resonance energy transfer revealed that both the number and the relative position of DNA sticky-ends play a significant role in the stability of the final assembly. As multivalent interactions are important factors in nature's delicate macromolecular systems, our quantitative analysis of the stability and cooperativity of a network of DNA sticky-end associations could lead to greater control over hierarchical nanostructure formation and algorithmic self-assembly.

INTRODUCTION

Biological systems contain a myriad of macromolecular structures formed through self-assembly of interacting molecular components (1). Emulation of biological self-assembly processes offers great potential for nanofabrication (2). In recent years, a number of research groups have begun developing nanofabrication methods based on DNA self-assembly (3–23). The chemical properties of DNA that allow it to successfully function as life's information carrier have been exploited for advances in the field of nanotechnology (24). The DNA molecule has attractive features for use in nanotechnology as a result of its nanoscale dimensions, its ability to form duplexes and other higher-order structures, and its combined stiffness and flexibility (25). The exceptional specificity of Watson-Crick hydrogen-bonding interactions allows the convenient programming of synthetic DNA via a simple four-letter alphabet.

The fabrication of a DNA nanostructure begins with the assembly of a collection of deliberately designed, single-stranded DNA molecules into branched DNA motifs, commonly referred to as DNA tiles. A diverse architectural toolbox of rigid, branched DNA nanostructural motifs that serve as ''molecular bricks'' has been developed (26). The most convenient way of bringing individual DNA tiles together to form higher-order structures is by sticky-end cohesion through complementary basepairing, where a sticky end is a short, single-stranded overhang that extends beyond the end of a double-stranded helical DNA molecule.

Despite the importance of inter-tile sticky-end interactions in structural DNA nanotechnology, very few studies of the effect of multivalency and strength of sticky-end cohesion have been performed. Particularly, research on the effect of varying the number and position of sticky ends on the thermodynamics of a multi-tile assembly is lacking. With an enhanced understanding of the thermal stability of a network of sticky-end associations, greater control over nanostructure formation and self-assembly may be achieved. For example, one of the main obstacles in achieving robust algorithmic DNA self-assembly is the presence of several types of errors (9): structural, nucleation, and growth errors have hampered the development of this field. It may be possible to reduce error rates by carefully tuning the kinetics and thermodynamics of assembly, and studies that provide such quantitative information could lead to better control over the self-assembly process.

Analysis of the thermodynamic stability of DNA architectures has frequently been carried out by way of melting temperature examination. The melting curves of DNA complexes provide a measure of the stability and cooperativity of internal interactions via the transition temperature, and the width of the transition, respectively. Melting curves of DNA complexes are most often acquired by exploitation of the hyperchromatic effect of nucleotides, through measurement of the absorption change (at 260 nm) of basepaired oligonucleotides upon thermal denaturation. There have been many reports on the melting temperatures of discrete DNA nanostructures (8,27). However, there have been very few reports on the thermal stability and dynamics of inter-tile sticky-end associations. This is because the amplitude of the absorbance change for the dissociation of sticky ends (usually only 5–10 nucleotides long) is overshadowed by the much larger absorbance change resulting from the dissociation of the core of the DNA tile (28). In addition, the existence of multiple intermediate states during the melting of a DNA tile makes the assignment of particular transitions to distinct structural changes very difficult. Additionally, ultraviolet-based melting measurements are restricted to

Submitted April 2, 2009, and accepted for publication May 6, 2009.

*Correspondence: yan_liu@asu.edu or hao.yan@asu.edu

Editor: David P. Millar.

0006-3495/09/07/0563/9 $2.00

doi: 10.1016/j.bpj.2009.05.013

final-product analysis, which constrains the ability to detect and optimize the self-assembly process.

Recently Sacca et al. developed a method to analyze the self-assembly of DNA nanostructures in real-time using temperature-dependent fluorescence resonance energy transfer (FRET) spectroscopy (29). In this method, the direct monitoring of the self-assembly process is enabled by the precise placement of a pair of FRET fluorophores on two constituent oligonucleotides of a DNA nanostructure. The interfluorophore distance changes as a result of temperature-dependent conformational changes. Correct assembly of the nanostructure upon cooling brings the FRET pair into close proximity and induces maximum FRET efficiency at low temperatures. In contrast, the complete dissociation of the nanostructure upon thermal melting results in separation of the FRET pair and induces minimal FRET efficiency at high temperatures. By monitoring the change of FRET efficiency with temperature, the equilibrium constant of the self-assembly process at each temperature can be obtained. In the case of reversible assembly and disassembly of a DNA nanostructure, application of the van 't Hoff's law yields the enthalpy and entropy changes of the assembly process.

Design

Herein the FRET-based method was used to systematically investigate the behavior and thermal stability of a series of sticky-end associations occurring between two multihelical DNA nanostructures, illustrated in Fig. 1 *A* (30). Two types of multihelical tiles, 4HX and 6HX, were used, differing only in the number of helices contained in each tile. Within each tile, the DNA helices are arranged parallel to adjacent helices and are joined with oligonucleotides that cross-over from one helix to its neighboring helices.

As shown in Fig. 1, two 4HX tiles (4HX-A and 4HX-B) capable of specifically associating to form heterodimers through 1–4 sticky-end connections were designed and constructed. Each of the 4HX tiles were formed from nine constituent DNA oligomers that self-assembled into the desired tiles when mixed together and annealed. The 3′ ends of the four helices were extended with six-nucleotide-long, single-stranded overhangs, which functioned as sticky ends for the tile-tile association (on the right side of tile A and the left side of tile B). The complementarities of the corresponding sticky ends on tile A and B are labeled with numbers (1 and 1′, etc.) and represented by different colors and shapes. The sequences of all of the sticky ends were designed to contain the same GC content. A systematic study of sticky-end associations between the tiles in the dimer assembly was carried out by analyzing a variety of combinations of number and position of sticky-end pairs. Fig. 1 *B* illustrates the different designs of the 4HX dimers labeled from #1 to #8. Between the tiles, the helical positions without sticky-end attachments

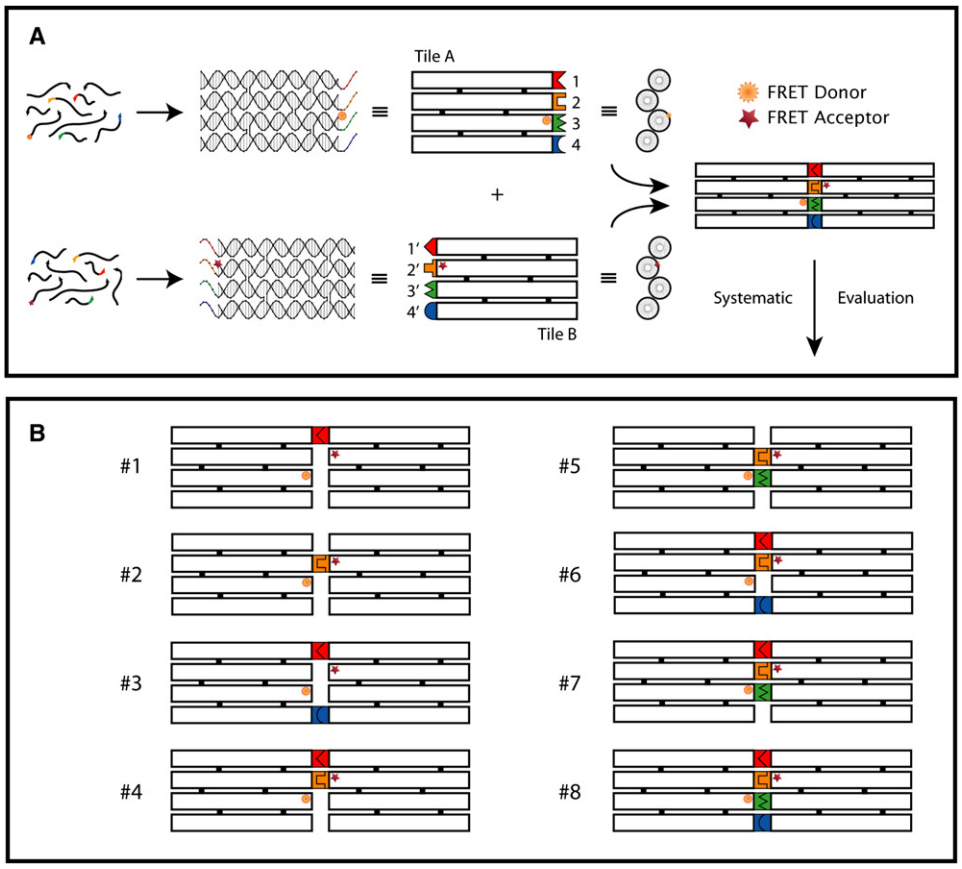

FIGURE 1 (*A*) Schematic representation of the labeling strategy used for the FRET thermal analysis of the self-assembly of DNA tile dimers. The FRET pair is Fluorescein (*orange sunburst*, donor) at the right end of helix 3 on tile A, and TAMRA (*red star*, acceptor) at the left end of helix 2 on tile B. Correct formation of the DNA tile dimer through sticky-end association (labeled by numbers and represented by different colors and complementary shapes) brings the FRET pair into proximity leading to efficient FRET. (*B*) Schematic representation of the collection of designs (#1–#8) for the 4HX dimers formed though numbers of sticky ends ranging from 1 to 4, with variable sticky-end positions.

were trimmed to be blunt ends to prevent them from interfering with dimer formation. Oligomers on the opposite (outer) end of the tiles contain a poly-thymine (T4) sequence extending outward to prevent the undesired, nonspecific association of tiles through blunt-end stacking, thus ensuring that the resulting assemblies are discrete dimers.

To rule out the possibility that base-stacking interactions between the tiles (at positions without sticky-end attachments) might have an influence on the experimental measurements, four thymines were added to the corresponding oligomers in control experiments (see the Supporting Material for details). The melting curves obtained for the standard and control samples were not substantially different, indicating that the end-to-end base stacking interactions in the designs here provided no significant contribution to the thermal stability of the dimers. It should be noted that there are approximately three full helical turns (31 basepairs) separating neighboring inter-tile crossover points, so that the two tiles in the dimer should lie within the same plane. However, for dimer assemblies connected by a single sticky-end association, tiles A and B may be positioned slightly out of plane, due to a twisting (underwinding) of the hybridized helical region of the connection. The effect of this twisting on the stability of these dimers will be discussed later.

Additionally, two 6HX tiles (6HX-A and 6HX-B) that are capable of forming heterodimers with a number of sticky-end connections ranging from one to six were also prepared. The 6HX tiles were formed from 14 constituent oligomers that self-assembled into the desired tile when mixed together and annealed. Similarly, selected 3′ ends of the six helices were extended with six-nucleotide-long complementary sticky ends to facilitate dimer formation. For 6HX tiles, the sequences of the sticky-end pairs were kept the same for designs with the same number of sticky-end connections. For example, for designs with one sticky-end connection the same sticky-end sequence was used for each of the six possible positions. Additionally, for designs with two sticky-end associations, two pairs of unique sticky-end sequences with the same GC content were used for each of the 15 possible arrangements. For the 6HX system, all possible combinations of number and position of sticky ends were constructed and analyzed (see the Supporting Material for detailed structure and sequences).

The thermal-stability of the various dimer assemblies was determined by the aforementioned FRET method. To enable the in situ monitoring of the self-assembly process by FRET spectroscopy, the A and B tiles of the heterodimer were labeled with a pair of fluorescent dyes. One constituent oligomer from tile A was labeled with a FRET donor, Fluorescein ($Ab_{max} = 495$ nm, $Em_{max} = 520$ nm) and one constituent oligomer from tile B was labeled with a FRET acceptor, TAMRA ($Ab_{max} = 559$ nm, $Em_{max} = 583$ nm). The fluorescent dyes were covalently attached to the corresponding oligomers on the 5′ end of strands not carrying a sticky end, on the third and second helical positions of tiles A and B, respectively (Fig. 1). All dimer constructions investigated shared the same pair of fluorescently-labeled oligomers. The distance between the two fluorophores in the final dimer assemblies is estimated to be ~3 nm for all constructs examined. When the individual DNA strands comprising each tile are annealed and assembled into the dimer superstructure, the FRET pair is brought into proximity and induces maximum FRET efficiency. The dissociation of the dimer superstructure results in separation of the FRET pair and leads to minimal FRET efficiency.

MATERIAL AND METHODS

Self-assembly of DNA nanostructures

All DNA strands used for assembly of nanostructures were purchased from Integrated DNA Technologies (www.idtdnacom) and purified by denaturing PAGE gel electrophoresis (6–10% acrylamide in 1× TBE buffer: 89 mM Tris base, 89 mM Boric acid, 2mM EDTA, pH 8.0) or HPLC for the dye-labeled DNA oligomers. Assembly of the individual tiles as well as the final superstructure was performed by mixing equimolar amounts of all the oligomers present in the structures at a final concentration ranging from 0.6 to 1 μM in 1× TAE Mg buffer (40 mM Tris base, 20 mM Acetic acid, 2 mM EDTA·Na_2·$12H_2O$, 12.5 mM $(CH_3COO)_2Mg·4H_2O$). The oligomer mixture was heated at 95°C for 5 min and cooled down to 25°C (~−0.1°C/min) using an automated real-time PCR thermocycler (Mx3005P; Stratagene, La Jolla, CA). The formation of self-assembled individual tiles as well as the final superstructure was demonstrated by nondenaturing PAGE (8% acrylamide in 1× TAE Mg buffer (40 mM Tris base, 20 mM Acetic acid, 2 mM EDTA·Na_2·$12H_2O$, 12.5 mM $(CH_3COO)_2Mg·4H_2O$; 150V, 20°C for 5 h) and FRET spectroscopy.

Fluorescence spectroscopy

The fluorescence thermal curves were measured in eight-well optical tube strips using a MX3005P real-time thermocycler (Stratagene). After mixing equimolar amounts of all oligomers present in the nanostructures (0.3 or 0.5 μM concentration in 1× TAE Mg buffer), 20 μL of each sample was pipetted into Stratagene optical tube strips and closed with Stratagene optical caps. The samples were heated to 95°C for 5 min, and upon excitation at 492 nm, the fluorescence emission of fluorescein (522 nm) was monitored while the temperature was reduced from 80°C to 25°C with a temperature gradient of −0.1°C/min. Heating cycles were performed in the same manner: after one cooling cycle the samples were held at 25°C for 10 min and upon excitation at 492 nm, the fluorescence emission was monitored while the temperature was increased from 25°C to 80°C with a temperature gradient of +0.1°C/min. All experiments were repeated at least in duplicate to ensure reproducibility. For all the nanostructures investigated, two samples were prepared with identical experimental conditions: One sample contained the donor on tile A and the acceptor on tile B (A^DB^A), whereas the second sample contained only the donor fluorophore on tile A and corresponding unlabeled oligomer on tile B (A^DB) as the reference. This scheme allowed for the measurement of the decrease in donor emission resulting from energy transfer to the TAMRA acceptor to calculate the FRET efficiency. This method also allowed for the variations in the donor's fluorescence as a result of changes in temperature to be taken into account. Analysis of the data illustrated variations in the FRET efficiency of the donor-acceptor pair during the self-assembly process.

RESULTS AND DISCUSSION

The proper formation of the AB tile dimers was confirmed by native polyacrylamide gel electrophoresis (see gel images in

the Supporting Material). The AB tile dimer constructs exhibited a distinct mobility as compared to that of the individual tiles.

The efficiency of energy transfer (E) was determined at each temperature according to

$$E(T) = 1 - \frac{I_{DA}(T)}{I_D(T)}, \quad (1)$$

where I_{DA} and I_D are, respectively, the fluorescence intensities of the FRET donor (Fluorescein) in the presence and absence of the FRET acceptor (TAMRA). Assuming the change in the fluorescence intensity of the donor is proportional to the formation of dimers containing the FRET pair, and that the system reaches equilibrium at each temperature as a result of the slow temperature gradient, the fraction of assembled dimer structures at any given temperature $\theta(T)$ is obtained by normalization of FRET efficiency as a function of temperature,

$$\theta(T) = \frac{E(T) - E_{min}}{E_{max} - E_{min}}, \quad (2)$$

where E_{min} represents the minimum FRET efficiency that occurs when the superstructure is completely dissociated, and E_{max} represents the maximum FRET efficiency that occurs when the superstructure is completely assembled. $\theta(T)$ gives information about the equilibrium shift of the reaction of A+B $\Leftrightarrow$ AB as a function of temperature: at E_{max}, all DNA tiles are fully assembled to form AB dimers, and therefore $\theta = 1$. In contrast, at E_{min}, all DNA strands are completely dissociated and therefore $\theta = 0$.

The intensity of fluorescence emission of the FRET donor in the presence and absence of the acceptor, I_{DA} and I_D, was obtained for each pair of samples. The raw data were plotted against temperature in the 25–80°C range and the heating and cooling profiles were superimposed (a typical sample is shown in Fig. 2 *A*). After determining the assembled fraction of dimers at each temperature using Eqs. 1 and 2, θ was also plotted against temperature with the heating and cooling profiles superimposed (Fig. 2 *B*). It is observed that the heating and cooling profiles for an individual construct followed each other closely with negligible hysteresis, especially for the normalized data (Fig. 2 *B*), indicating the reversibility of the dimer formation and dissociation processes.

The raw fluorescence intensity data (Fig. 2 *A*) reflects the assembly process for a typical sample. During the assembly (cooling) process, the A^DB^A constructs exhibited a minor and gradual increase in the donor emission as a result of changes in temperature, in addition to two sharp decreases in the donor emission at the characteristic transition temperatures, at ~62°C and ~52°C, respectively. In contrast, the A^DB reference sample (donor only) exhibited two sharp transitions—a similar decrease at ~62°C, but then an increase at ~52°C, in the opposite direction of the change for the A^DB^A sample. For both samples, the decrease in donor emission at ~62°C corresponds to the formation of the individual DNA tiles from their constituent strands during the cooling phase. It is known that for a fluorescein dye conjugated to DNA, the fluorescence quantum yield decreases as the DNA transforms from single-stranded to double-stranded, possibly due to weak, noncovalent interactions of the dye with the DNA helix (31). This transition, occurring in both samples, has a similar magnitude of change, thus a subtraction operation using Eq. 1 will cancel out this transition. For both samples, the transition at ~52°C corresponds to the dimer

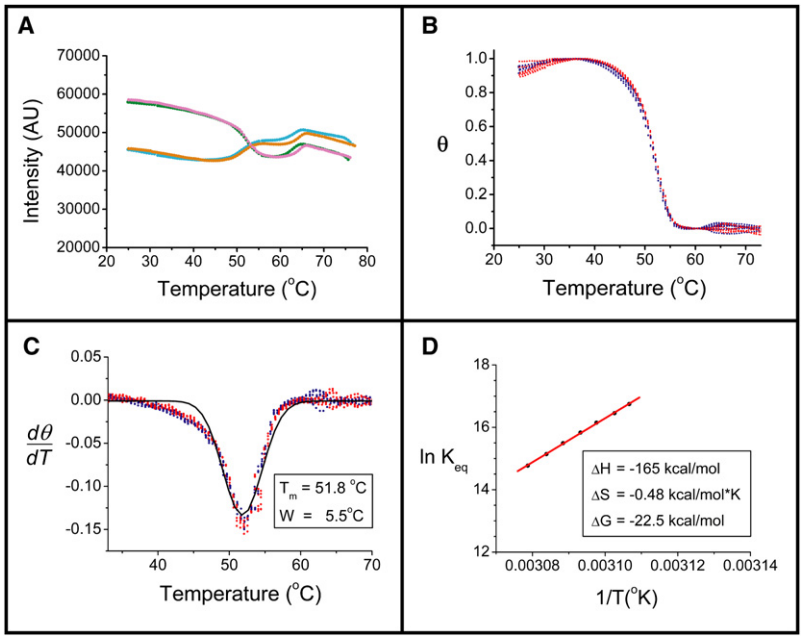

FIGURE 2 Illustration of data analysis for a typical sample (design #6 as shown in Fig. 1 *B*). (*A*) The raw data (fluorescence intensity versus temperature) are read directly from the real-time PCR thermocycler detector, with the heating and cooling curves for the A^DB^A sample in orange and cyan, respectively, and the heating and cooling curves for A^DB in magenta and olive, respectively. (*B*) The plot of normalized FRET efficiency, θ, as a function of temperature. Eight profiles for both heating (*red*) and cooling (*blue*) are plotted together here, exhibiting negligible hysteresis. In this figure only one transition, at ~52°C, is observed. (*C*) The first derivative of the profiles in panel *B*, $d\theta/dT$, versus temperature is plotted, and a Gaussian fit yields the transition temperature and the width of the transition (again, eight profiles are superimposed). (*D*) A linear fit of the van 't Hoff plot generates the changes of enthalpy (ΔH), entropy (ΔS), and thereby the free energy change (ΔG).

formation. The increase of PL for the A^DB sample may result from the formation of sticky-end associations, expelling the donor fluorophore out of the DNA helix by electrostatic or steric repulsion, thereby yielding a higher fluorescence emission. On the other hand, the decrease of the donor emission at ~52°C for the dimer containing the FRET pair is a result of the FRET donor and acceptor being forced into close proximity, inducing maximum FRET efficiency, thus decreasing the donor emission. The subtraction of the two curves and normalization according to Eqs. 1 and 2 results in the curves shown in Fig. 2 *B*, which exhibit only one transition that is directly related to the dimer formation.

The transition temperature (melting temperature) was obtained by fitting the first derivative of θ versus temperature with a Gaussian function, $Y = Y_0 + \frac{A}{w\sqrt{\pi/2}} e^{-2\left(\frac{T-T_m}{w}\right)^2}$, where T_m is the midpoint of the transition temperature, and w is ~0.849 × the full width of the peak at half-height (Fig. 2 *C*). All the constructs analyzed showed a reversible thermal transition, allowing the application of the van 't Hoff law.

For van 't Hoff analysis, the variation of the equilibrium constant (K_{eq}) with temperature is used to obtain the enthalpy and entropy changes of the complex formation. The equilibrium constant of dimer formation can be expressed as a function of the assembled fraction of dimers at equilibrium,

$$K_{eq} = \frac{\theta}{C_0(1-\theta)^2}, \quad (3)$$

where C_0 is the molar concentration of the individual tiles in the mixture, and θ is the assembled fraction of the dimer structure at equilibrium assuming a two-state transition. The following equation describes K_{eq} as a function of temperature,

$$\ln K_{eq} = \frac{-\Delta H}{RT} + \frac{\Delta S}{R}, \quad (4)$$

where ΔH is the enthalpy change and ΔS is the entropy change. Plots of $\ln K_{eq}$ versus $1/T$ in the temperature range of the transitions were linear, indicating that ΔH and ΔS are temperature-independent (Fig. 2 *D*). The van 't Hoff enthalpy and entropy changes for the reversible thermal transitions allowed the calculation of changes in free energy for the assembly process using the Gibbs equation,

$$\Delta G = \Delta H - T\Delta S, \quad (5)$$

where T is 298 K (25°C).

The results of data analysis for the 4HX tile constructions are listed in Table 1. Analysis of the experimental results reveals that changes in the number and position of sticky ends lead to significant differences in the thermal stability of superstructure associations.

First of all, there is a clear trend of enhanced thermal-stability with increasing numbers of sticky ends for both 4HX and 6HX tiles. This increase in melting temperature is accompanied by a more negative free energy change. Fig. 3 summarizes the dramatic effect of increasing the number of sticky-end associations on melting temperature and free energy changes for the 4HX system. For 4HX dimers, there is a considerable increase in melting temperature, by ~13°C, when the number of sticky ends between tiles is changed from one to two. Previous studies have qualitatively shown that larger and more stable arrays are generated using two sticky-end associations between constituent tiles as compared to one sticky-end association (32). The results of the current study provide direct quantitative confirmation of this phenomenon. Increasing the number of sticky-end associations between the 4HX tiles from two to three further elevates the melting temperature of the dimer superstructure by another ~8°C, to above 50°C. It is notable that increasing the number of sticky-end associations further from three to four does not result in as dramatic an increase in melting temperature. The same trends were observed in the amplitude of the free energy changes (Fig. 3 *B*). Rather than a purely additive effect, the number of sticky-end associations between the two tiles reaches a saturation point when all of the sticky ends available are fully utilized. The deviation from a linear dependence of the increase of the melting temperature and free energy change on the number of sticky ends may be a result of the less-than-ideal cooperativity of binding. It seems that for the multihelical tiles ($n >= 4$), addition of the last sticky end (from $n-1$ to n) does not contribute significantly to the overall thermal stability of

TABLE 1 Thermostability data for the 4HX DNA dimers associated through various combinations of number and position of sticky-end interactions

No. of sticky ends	Positions of sticky ends	T_m (°C)	$w/2$ (°C)	$-\Delta H$ (kcal/mol)	$-298\Delta S$ (kcal/mol)	ΔG (kcal/mol)
1	1	28.6 ± 0.8	5.5 ± 0.8	85.5 ± 26	75.1 ± 26	−10.5 ± 0.5
	2	34.4 ± 0.2	5.5 ± 0.4	87.5 ± 5.5	75.7 ± 5.4	−11.7 ± 0.3
2	1, 4	42.0 ± 0.8	3.5 ± 0.4	82.4 ± 13	69.1 ± 12	−13.3 ± 0.8
	2, 3	44.6 ± 2.2	4.9 ± 0.4	105.1 ± 7.8	89.7 ± 7.5	−15.3 ± 0.5
	1, 2	46.5 ± 1.2	4.0 ± 0.9	116.6 ± 19	99.8 ± 17	−16.8 ± 1.7
3	1, 2, 4	51.8 ± 0.2	2.7 ± 0.1	166.4 ± 15	143.9 ± 14	−22.5 ± 1.3
	1, 2, 3	53.3 ± 0.5	3.0 ± 0.2	148.2 ± 11	126.4 ± 10	−21.7 ± 1.1
4	1, 2, 3, 4	54.7 ± 0.9	2.9 ± 0.3	143.7 ± 27	121.6 ± 25	−21.9 ± 2.5

Structural schemes for these samples are shown in Fig. 1 *B*. The ± values are the standard deviations of the average for both the heating and cooling curves from multiple repeats (12–18 curves for each sample), representing the uncertainty of the experimental measurements.

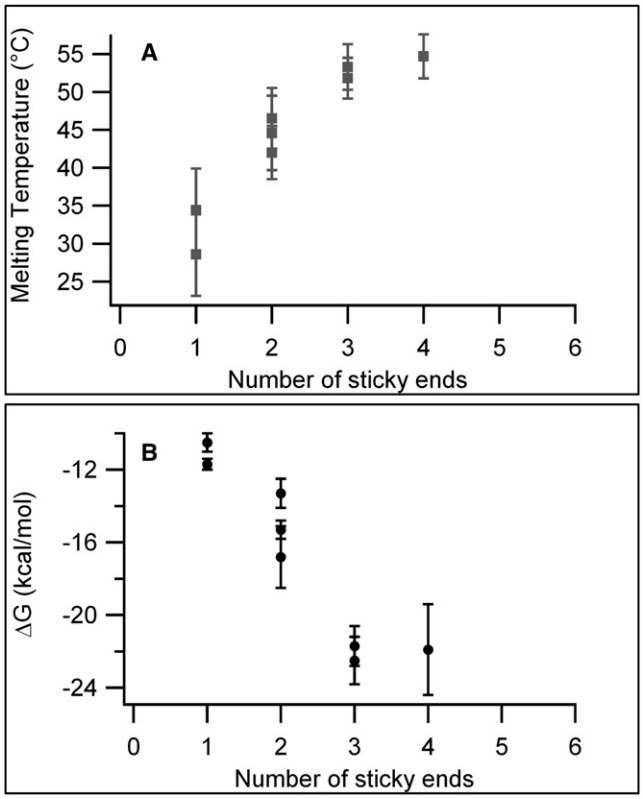

FIGURE 3 (*A*) Transition temperature and (*B*) free energy change versus the number of sticky ends for the 4HX dimers. In panel *A*, the error bars reflect the width of the transition temperature ($w/2$), and in panel *B*, the error bars reflect the standard deviation of the calculated free energy changes. The variations in the different data points for the same number of sticky ends (one, two, and three sticky ends) reveal the positional effects of sticky-end placement.

the construct. This could be the result of more negative entropy changes, given that the degrees of freedom for the vibrational and rotational motions of the tile dimer decrease when more of the helical ends are employed for the association of two tiles.

The width of the transition reflects the degree of cooperativity of the assembly: the sharper (corresponding to a narrow temperature range) the transition is, the more cooperative the assembly process is. Here the cooperativity is defined vaguely as the number of species involved in the assembly. The error bar in Fig. 3 *A* represents the width of the transition, which grows smaller as the number of sticky ends involved increases, consistent with the notion that multivalency improves cooperativity.

The melting temperature data corresponding to various numbers of sticky-end associations for both the 4HX (*squares*) and 6HX systems (*circles*) are superimposed in Fig. 4. There are considerable variations in the melting temperatures for dimers with the same number of sticky ends at different positions. The variation in the melting temperature for designs with the same number of sticky ends exceeds the uncertainty of the measurements indicating the differences are real, not merely a result of experimental errors.

On average, 6HX dimers exhibited overall lower melting temperatures than 4HX dimers with the same number of sticky-end associations. This can be explained in analogy to the anharmonic vibration model of a chemical bond between two atoms: with severe elongation of the bond (sticky-end basepairing), the dimer structure is doomed to dissociate. This is the result of the bond weakening that occurs when the bond distance is far removed from the equilibrium distance, i.e., the normal length of a B-type DNA duplex with six basepairs, stacked nearly in parallel with a plane gap of 0.34 nm. 4HX and 6HX dimers with the same number of sticky-end associations can be considered to have the same force constant (k). Consequently, dimers formed from larger tiles (6HX) will have a lower vibrational resonance frequency, and will dissociate at a lower temperature than the dimers formed from the smaller tiles (4HX). The melting phenomenon of crystalline structures was studied by Einstein a hundred years ago (33). He derived that a crystalline lattice with a lower characteristic vibrational frequency will have a lower melting temperature than a lattice with a higher

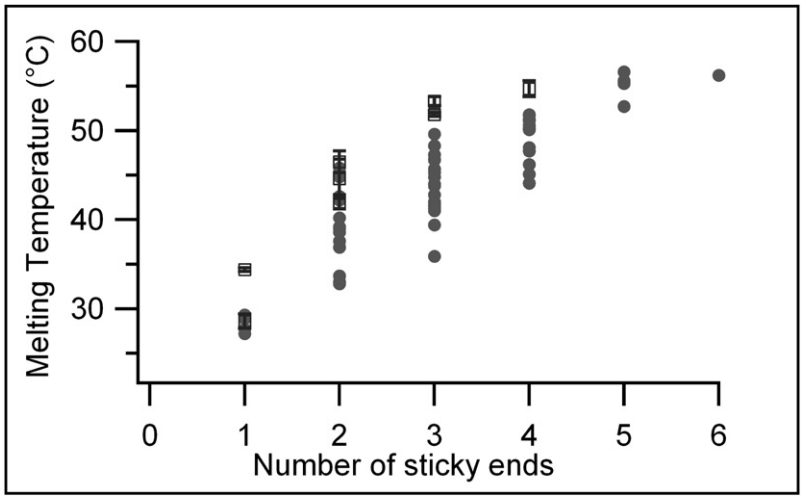

FIGURE 4 Effect of the number of sticky-end associations on the melting temperature of 4HX dimers (*squares*) as compared to 6HX dimers (*circles*). The error bars on the 4HX data are the standard deviations, reflecting the repeatability of the melting temperature measurements using 4–6 repeats for each sample including both heating and cooling. The error bars for the 6HX data are not included to make the figure more readable. The range of the transition temperatures for designs with the same number of sticky ends is generally wider than the error of the measurements, reflecting the dramatic positional effects of sticky-end placement.

characteristic vibrational frequency. The corresponding melting temperature is referred to as the Einstein temperature. Our observations are in agreement with the Einstein theory.

The positions of the sticky-end connections have a distinct influence on the thermal-stability of the dimer structure, especially for the 6HX system, which has a large number of different positional combinations available. It is noted that the sequences of the sticky ends for designs with the same number of associations (e.g., 1, 2, and 3 sticky ends) are all the same for the 6HX system, thus the sizeable variations in the melting temperatures observed at different positions can only be explained by the positional effects described below.

First, the absolute position of sticky ends relative to the multihelical tile has a profound effect on the thermal stability of the tile-to-tile connection (Fig. 5 *A*). Experimental results for designs with one sticky-end association indicate that constructs with sticky ends located at central helical positions (positions 2–5) are significantly more stable than those with sticky ends located at the terminal positions (positions 1 or 6). The same trend was observed for the 6HX dimer constructs with two adjacent sticky-end associations. Fig. 5 *B* demonstrates the lower melting temperature resulting from a pair of terminal sticky-end positions (pair position 1-2, or 5-6) as compared to a pair of central sticky-end positions (pair position 2-3, 3-4, or 4-5).

The effects of the absolute positions of sticky ends on the dimer stability can be explained by considering the repulsive forces that exist between the multihelical tiles. Constructs in which the sticky end(s) are located on terminal helices experience repulsive forces between the two tiles that do not pass through the center-of-mass of the system. This generates a torque, leading to distortions of the helix or helices involved in the association. Bending (in plane of the tiles) and twisting (out of plane of the tiles) of the helical region corresponding to the sticky ends could effectively weaken the strength of the complementary basepair hydrogen-bond interactions and disrupt base-stacking interactions between the neighboring basepairs. The in-plane bending effect is expected to be less dramatic for constructs with sticky ends located at central helical positions due to a near-symmetric distribution of charge and mass, thus resulting in less of a reduction of thermal stability. The out-of-plane twisting effect should be less important for any number of sticky-end connections greater than one.

Second, it must be noted that the positional effect is not perfectly symmetric, e.g., when comparing the designs with two sticky ends on terminal helices, sticky ends at positions 1 and 2 yield a higher melting temperature than those at positions 5 and 6. This may be due to the fact that the structural strain of the tile is not evenly distributed, resulting in a distortion of the inner, parallel helices so that the tile structure is not as symmetric as illustrated in the model. The melting of the dimer can be thought of as an unzipping of the sticky-end connections, with the separation of tile A from tile B beginning from the nick points between sticky ends. At the same time the melting of the individual tiles starts from the ends of the helices with no sticky-end connections. In this context it is important to note that the FRET donor and acceptor fluorophores are located on the second and third helices of the dimer structure. When there are no sticky ends extended from helices where the acceptor and donor molecules are attached, the donor and acceptor molecule could be separated before the tiles are fully dissociated at the sticky ends. Consequently, dimers that have sticky-end connections far away

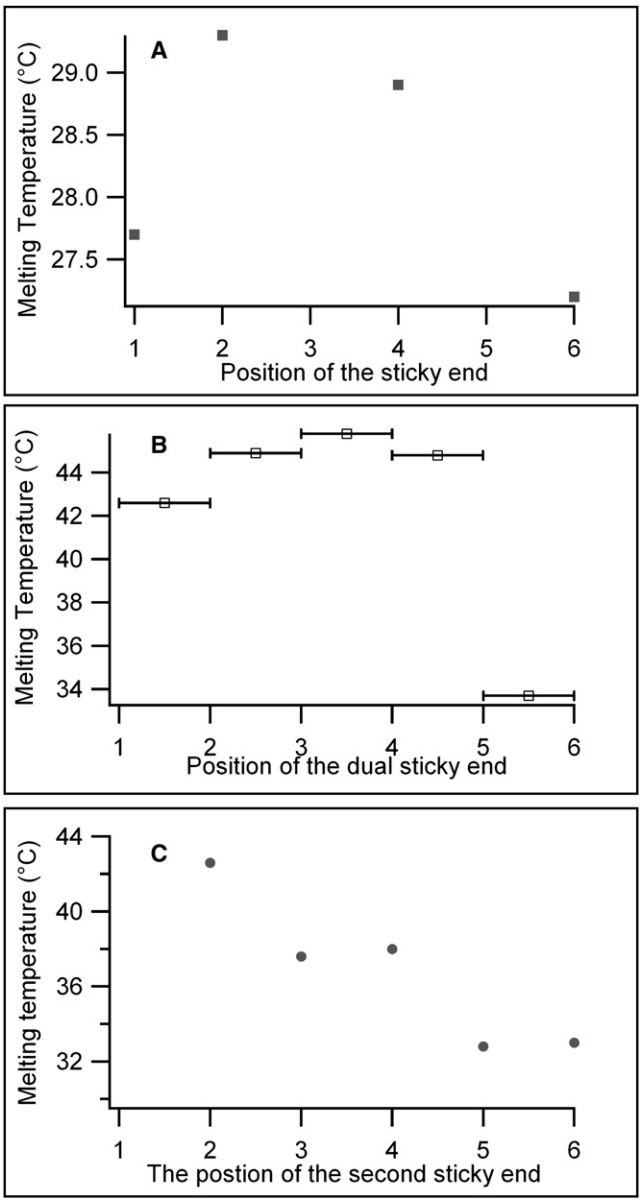

FIGURE 5 (*A*) Effect of absolute position of one sticky end on the thermal stability (represented by T_m) of 6HX dimers. (*B*) The effect of absolute position of two adjacent sticky ends on the T_m of 6HX dimers. The horizontal bars in the figure indicate the adjacent positions of the two sticky ends. (*C*) The effect of relative position of two sticky ends on T_m of 6HX dimers. The horizontal axis is the position of the second sticky end, where in all cases the first sticky end is positioned on helix 1.

from the donor and acceptor molecule positions could show relatively lower melting temperatures. This can also partially explain the asymmetric positional effect.

Furthermore, for multi-sticky-end associations ($n \geq 2$), the relative position of sticky ends with respect to each other also results in a significant effect on the thermal stability of the tile-to-tile association. Experimental results show that for two sticky-end associations, the wider the gap between the sticky ends, the less stable the dimer. Fig. 5 *C* displays the effect of relative position of sticky ends on dimer melting temperature. The melting temperature for a 6HX dimer with two sticky ends located at the two extreme helical positions (positions 1 and 6) is 10°C lower than that of a dimer with two sticky ends adjacent to one another (positions 1 and 2). The previously mentioned effect of absolute sticky-end position on thermal stability is further illustrated with the reduction of another 3°C in the melting temperature of dimers with adjacent sticky ends at terminal helical positions (e.g., positions 1 and 2) as compared to those with adjacent sticky ends at central positions (e.g., positions 3 and 4), as shown in Fig. 5 *B*. The same trend holds true for 6HX constructs with three sticky-end associations; three sticky ends adjacent to one another, located at central positions of the tile, result in constructs with higher melting temperatures than those with gaps between the sticky ends.

These differences are not only reflected in the changes of the melting temperatures, but also in the enthalpy and entropy changes (Table 1). Increasing the number of sticky-end associations from 1 to 2 is expected to double the enthalpy change, but our results show that this is not the case, especially for situations in which the sticky ends are located far apart. From Table 1 it is noted that rather than an increase, there is a small decrease in the value of the enthalpy change upon addition of a second sticky-end at position 4 to a dimer with a sticky-end already at position 1. Nevertheless, this additional sticky-end results in a higher melting temperature (from 28 to 42°C) with a more negative free energy change. The much lower melting temperature for one sticky end located at position 1 can be explained by the weakening of the sticky-end association by two kinds of relative motions of the two tiles in the dimer: an out-of-plane motion that disrupts the normal helical twist and an in-plane rotational motion that disrupts the parallel base-stacking. The out-of-plane motion is eliminated for the dimers formed through two sticky ends. The in-plane motions still exist as the two sticky ends alternate in the stretching and compressing phases. However, as the two sticky ends are adjacent to one another, their motions are restricted and must be coordinated to avoid any steric hindrance. Since the sticky ends positioned far apart from one another experience more rotational freedom, this results in a smaller loss of entropy and a smaller enthalpy change. The free energy change depends on the relative contributions of these two terms. For example, for the 4HX dimers, when the sticky-end connection is changed from one sticky end at position 1 to two sticky ends at positions 1 and 2, the most significant contribution to the more negative free energy change comes from a large change in enthalpy. In contrast, when the sticky-end connection is changed from position 1 to positions 1 and 4, the greater contribution to the more negative free energy change comes from a less negative entropy change, with a negligible difference in the enthalpy change.

CONCLUSION

In summary, we have designed a set of DNA tiles for use as a model system to study the thermal behavior of multivalent DNA hybridization that would otherwise be difficult to achieve using simple DNA duplexes. The real-time monitoring of tile-to-tile associations revealed that both the number and the relative position of sticky-end connections play significant roles in the stability of the final assembly. The differences in the melting temperature and free energy, resulting from various geometric arrangements of sticky ends, provide more options for the deliberate control of self-assembling DNA nanostructures. For example, one could utilize these parameters to design DNA tile sets for algorithmic self-assembly and/or hierarchical self-assembly based on the cooperative interactions determined by multivalent associations. One may also be able to design and produce kinetically trapped products by engineering the sticky-end pairs. Nevertheless, more research must to be done to reveal the fundamental aspects of intricate DNA self-assembly systems that may in turn provide insights into other macromolecular assembly processes found in nature. For example, measurements of enthalpy by calorimetry may be used in the future to gain additional insights on such systems.

SUPPORTING MATERIAL

Six figures are available at http://www.biophysj.org/biophysj/supplemental/S0006-3495(09)000975-8.

Other supporting information is available on the DNA sequences used in this work, gel electrophoresis characterization of the DNA tiles, raw data, and additional analysis from the real time FRET experiments. This material is available free of charge via the Internet at http://pubs.acs.org.

We thank Prof. Shengli Zou for helpful discussion on the physical model of the system.

The authors thank the financial supports from the National Science Foundation and Army Research Office to Y.L.; and Air Force Office of Scientific Research, Office of Naval Research, the National Science Foundation, the Alfred P. Sloan Fellowship, Army Research Office, and the National Institutes of Health to H.Y.; and Technology and Research Initiative Fund funds from Arizona State University to H.Y. and Y.L.

REFERENCES

1. Klug, A. 1994. Macromolecular order in biology. *Philos. Trans. R. Soc. Lond. A.* 348:167–178.
2. Van Workum, K., and J. F. Douglas. 2006. Symmetry, equivalence, and molecular self-assembly. *Phys. Rev. E Stat. Nonlin. Soft Matter Phys.* 73:031502.

3. Seeman, N. C. 1982. Nucleic acid junctions and lattices. *J. Theor. Biol.* 99:237–247.
4. Winfree, E., F. Liu, L. A. Wenzler, and N. C. Seeman. 1998. Design and self-assembly of two-dimensional DNA crystals. *Nature.* 394:539–544.
5. Chen, J. H., and N. C. Seeman. 1991. Synthesis from DNA of a molecule with the connectivity of a cube. *Nature.* 350:631–633.
6. Yan, H., S. H. Park, G. Finkelstein, J. H. Reif, and T. H. LaBean. 2003. DNA-templated self-assembly of protein arrays and highly conductive nanowires. *Science.* 301:1882–1884.
7. Shih, W. M., J. D. Quispe, and G. F. Joyce. 2004. A 1.7-kilobase single-stranded DNA that folds into a nanoscale octahedron. *Nature.* 427:618–621.
8. Goodman, R. P., I. A. Schaap, C. F. Tardin, C. M. Erben, R. M. Berry, et al. 2005. Rapid chiral assembly of rigid DNA building blocks for molecular nanofabrication. *Science.* 310:1661–1665.
9. Rothemund, P. W., N. Papadakis, and E. Winfree. 2004. Algorithmic self- assembly of DNA Sierpinski triangles. *PLoS Biol.* 2:2041–2053.
10. Rothemund, P. W. K. 2006. Folding DNA to create nanoscale shapes and patterns. *Nature.* 440:297–302.
11. Aldaye, F. A., and H. F. Sleiman. 2007. Modular access to structurally switchable 3D discrete DNA assemblies. *J. Am. Chem. Soc.* 129:13376–13377.
12. He, Y., T. Ye, M. Su, C. Zhang, A. E. Ribbe, et al. 2008. Hierarchical self- assembly of DNA into symmetric supramolecular polyhedra. *Nature.* 452:198–202.
13. Le, J. D., Y. Pinto, N. C. Seeman, K. Musier-Forsyth, T. A. Taton, et al. 2004. DNA-templated self-assembly of metallic nanocomponent arrays on a surface. *Nano Lett.* 4:2343–2347.
14. Zhang, J., Y. Liu, Y. Ke, and H. Yan. 2006. Periodic square-like gold nanoparticles arrays templated by self-assembled 2D DNA nanogrids on a surface. *Nano Lett.* 6:248–251.
15. Zheng, J., P. E. Constantinou, C. Micheel, A. P. Alivisatos, R. A. Kiehl, et al. 2006. Two-dimensional nanoparticles arrays show the organization power of robust DNA motifs. *Nano Lett.* 6:1502–1504.
16. Sharma, J., R. Chhabra, Y. Liu, Y. Ke, and H. Yan. 2006. DNA-templated self-assembly of two-dimensional and periodical gold nanoparticles arrays. *Angew. Chem. Int. Ed.* 45:730–735.
17. Sharma, J., Y. Ke, C. Lin, R. Chhabra, Q. Wang, et al. 2008. DNA-tile-directed self-assembly of quantum dots into two-dimensional nanopatterns. *Angew. Chem. Int. Ed.* 47:5157–5159.
18. Williams, B. A. R., K. Lund, Y. Liu, H. Yan, and J. C. Chaput. 2007. Self- assembled peptide nanoarrays: an approach to studying protein-protein interactions. *Angew. Chem. Int. Ed.* 46:3051–3054.
19. He, Y., Y. Tian, A. E. Ribbe, and C. Mao. 2006. Highly connected two-dimensional crystals of DNA six-point-stars. *J. Am. Chem. Soc.* 128: 12664–12665.
20. Liu, Y., C. Lin, H. Li, and H. Yan. 2005. Aptamer-directed self-assembly of protein arrays on a DNA nanostructure. *Angew. Chem. Int. Ed.* 44:4333–4338.
21. Malo, J., J. C. Mitchell, C. Venien-Bryan, J. R. Harris, H. Wille, et al. 2005. Engineering a 2D protein-DNA crystal. *Angew. Chem. Int. Ed.* 44:3057–3061.
22. Gothelf, K. V., and T. H. LaBean. 2005. DNA-programmed assembly of nanostructures. *Org. Biomol. Chem.* 3:4023–4037.
23. Feldkamp, U., and C. M. Niemeyer. 2006. Rational design of DNA nanoarchitectures. *Angew. Chem. Int. Ed.* 45:1856–1876.
24. Seeman, N. C., and P. S. Lukeman. 2005. Nucleic acid nanostructures: bottom-up control of geometry on the nanoscale. *Rep. Prog. Phys.* 68:237–270.
25. Seeman, N. C. 2003. DNA in a material world. *Nature.* 421:427–431.
26. Lin, C., Y. Liu, S. Rinker, and H. Yan. 2006. DNA tile based self-assembly: building complex nanoarchitectures. *ChemPhysChem.* 7:1641–1647.
27. LaBean, T. H., H. Yan, J. Kopatch, F. Liu, E. Winfree, et al. 2000. Construction, analysis, ligation, and self-assembly of DNA triple crossover complexes. *J. Am. Chem. Soc.* 122:1848–1860.
28. Schulman, R., and E. Winfree. 2007. Synthesis of crystals with a programmable kinetic barrier to nucleation. *Proc. Natl. Acad. Sci. USA.* 104:15236–15241.
29. Sacca, B., R. Meyer, U. Feldkamp, H. Schroeder, and C. M. Niemeyer. 2008. High-throughput, real-time monitoring of the self-assembly of DNA nanostructures by FRET spectroscopy. *Angew. Chem. Int. Ed.* 47: 2135–2137.
30. Ke, Y., Y. Liu, J. Zhang, and H. Yan. 2006. A study of DNA tube formation mechanisms using 4-, 8-, and 12-helix DNA nanostructures. *J. Am. Chem. Soc.* 128:4414–4421.
31. Sjoback, R., J. Nygren, and M. Kubista. 1998. Characterization of fluorescein-ligonucleotide conjugates and measurement of local electrostatic potential. *Biopolymers.* 46:445–453.
32. Ding, B., R. Sha, and N. C. Seeman. 2004. Pseudohexagonal 2D DNA crystals from double crossover cohesion. *J. Am. Chem. Soc.* 126:10230–10231.
33. Cohen-Tannoudji, C., B. Diu, and F. Laloe. 1977. Quantum Mechanics, 2nd ed., Vol. 1. Wiley, New York.